ELSEVIER

Thin Solid Films 419 (2002) 124–136

thin solid films

www.elsevier.com/locate/tsf

GRANFILM: a software for calculating thin-layer dielectric properties and Fresnel coefficients

Rémi Lazzari[a,b,*], Ingve Simonsen[a,c]

[a]*Laboratoire Mixte CNRS/Saint-Gobain, 39 Quai Lucien Lefranc BP 135, 93303 Aubervilliers, France*
[b]*CEA-Grenoble, DRFMC/SP2M/IRS, 17 Rue des Martyrs, 38054 Grenoble Cedex 09, France*
[c]*NORDITA, Blegdamsvej 17, DK-2100 Copenhagen, Denmark*

Received 12 July 2002; received in revised form 19 July 2002; accepted 22 July 2002

Abstract

This paper describes new software—called GRANFILM—for computing linear optical coefficients for surfaces and thin layers. The underlying theory relies on the treatment of the electromagnetic boundary conditions at the surface using the notions of integrated electromagnetic excess fields and surface susceptibilities. Any type of Fresnel quantities (reflection, transmission, absorption or ellipsometric coefficients) and dielectric coefficients (energy electron loss cross-section) can be computed by this software for various kinds of surface morphology: thin continuous films, island layers made of truncated spheres or spheroids, or rough surfaces. The only restriction on the morphology is that the thickness of the surface perturbed layer is much smaller than the optical wavelength. GRANFILM covers most of the material developed by Bedeaux and Vlieger in the recently published book 'Optical Properties of Surfaces' (Imperial College Press, London, 2001).

PACS: 78.20.Bh; 78.66.-w; 68.55.-a; 73.20.Mf

Keywords: Optical properties; Optical spectroscopies; Surface plasmons; Surface roughness

1. Introduction

The use of optical techniques is widespread in the fields of thin film growth and surfaces as a characterisation tool, as well as for probing the dielectric properties of matter. For instance, ellipsometric measurements are performed daily in the semiconductor, glass and coatings industries in order to monitor the growth process of thin films. The most common measurements involve the layer thickness monitoring or the control of the composition of the layer through its dielectric properties. On a more fundamental point of view, despite its strong penetration depth, light is often used as a surface-sensitive probe [1–4] by enhancing the surface/volume signal thanks to experimental set-ups such as surface differential reflectance spectroscopy (SDRS) or reflectance anisotropy spectroscopy (RAS). Some fruitful information on the dielectric behaviour of surfaces can often be obtained by measuring Fresnel coefficients such as reflection, transmission or absorption. In such measurements, the influence of the layer properties, and more importantly, its morphology, is of prime interest. However, such information is difficult to take fully into account at the theoretical level. Solving the Maxwell equations in a spatial region containing an interface between two bulk media requires a precise idea of the nature of the boundary conditions that are satisfied by the electromagnetic fields. For complicated interfaces, such as randomly rough surfaces or granular thin films, i.e. islands of nm-size supported by a substrate, this might not be a trivial task. When the latter are made of small metallic particles, plasmon absorption modes [5,6], usually called 'Mie resonances', can be excited by visible light. These modes strongly affect the Fresnel coefficients in a way depending tremendously on the particle morphology [5].

These observations, among others, motivated Bedeaux and Vlieger in the early 1970s to try to tackle the

*Corresponding author. Tel.: +33-4-38785761; fax: +33-4-38785138.

E-mail addresses: lazzari@drfmc.ceng.cea.fr (R. Lazzari), ingves@nordita.dk (I. Simonsen).

0040-6090/02/$ - see front matter
PII: S0040-6090(02)00679-X

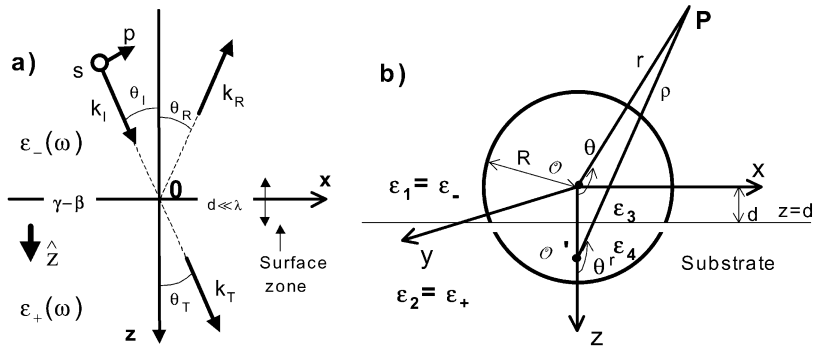

Fig. 1. (a) Reflection and transmission of an incident wave on a surface characterised by its surface susceptibilities β, γ. The perturbed surface layer of thickness *d* smaller than the wavelength λ separates two bulk media of dielectric constants ε_+, ε_-. (b) Truncated sphere geometry used to compute the island polarisability.

difficult problem of the optical response of surfaces. The basic idea of their approach was to use a perfectly flat surface as a starting point of the theory and to describe the role of any type of perturbation through so-called electromagnetic excess fields. These excess fields, as shown below, are nothing other than the difference between the bulk extrapolated fields and the real fields. The boundary conditions for the bulk fields, or in others words the jump of these quantities at the dividing surface, which drive all the Fresnel coefficients, are given in terms of the integrated excess fields perpendicular to the surface. For a perturbed layer, for which the thickness is negligible compared to the optical wavelength, those quantities can be interconnected by introducing coefficients called surface susceptibilities, which characterise the optical response of the surface. These closure relations are a kind of generalisation, applied to surfaces, of the link between displacement or induction fields and electric or magnetic fields. Since all the Fresnel coefficients can be expressed in terms of these surface susceptibilities, the main task consists of calculating these coefficients for the appropriate geometry.

The goal of GRANFILM is to calculate such coefficients and the associated measurable Fresnel quantities for various surface layer geometries. GRANFILM is free, open-source software available for the scientific community at http://www.phys.ntnu.no/~ingves/Software/GranularFilm/; the program can be used freely and the source codes can also be modified by the user to fit his/her needs.

This paper is organised as follows. In the first part, the theoretical bases of GRANFILM are briefly reviewed for various geometries frequently encountered in practical applications. The second part of the paper is devoted to the use of GRANFILM, illustrated by a case study consisting of a metallic island layer on a dielectric substrate. The influence of the dielectric properties of both the substrate and the metal are reviewed. In particular, in the case of islands, it is stressed that the model is able to obtain the main underlying features of the surface response, such as the excitation of multipolar absorption modes.

2. Theoretical background: excess fields and surface susceptibilities

The aim of this section is to summarise briefly the main elements needed in order to understand the models of excess fields and surface susceptibilities used in the description of the optical behaviour of surfaces. A full and complete discussion can be found in the original literature [7].

2.1. The integrated excess quantities and the surface susceptibilities

From an electromagnetic point of view, a surface is defined as a discontinuity between two half-infinite media with different (bulk) dielectric and/or magnetic properties (see Fig. 1a). However, when the surface is far removed from that assumed in the classic Fresnel theory, i.e. a sharp boundary between two media, the calculation of the reflection or transmission coefficients at the surface becomes increasingly complex. The reason for this difficulty is the complicated behaviour of the dielectric function perpendicular to the interface. Such a situation is encountered for rough surfaces or granular thin films in which a foreign material is distributed in small islands on top of a substrate.

Since the early 1970s, Bedeaux and Vlieger [7–12] have developed a formalism based on the notion of excess quantities. This approach does not require exact knowledge of the behaviour of the electromagnetic fields close to the surface for calculation of the Fresnel coefficients. These excess fields are defined as the difference between the real fields and the bulk fields extrapolated to the surface. For instance, in the case of the electric field $E(r)$, the definition of the excess quantity $E_{ex}(r)$ is:

$$E_{ex}(r) = E(r) - E^{-}(r)\theta(-z) - E^{+}(r)\theta(z) \quad (1)$$

where $\theta(z)$ is the Heaviside function and the superscripts $\pm$ are used to indicate the region above $(+)$ or below $(-)$ the reference surface $z=0$ (see Fig. 1a). The dependence upon the optical frequency ω is implicitly included in the notation. From this definition, it follows that the excess field is only significant close to the surface, since $E(r,\omega) \to E^{\pm}(r,\omega)$ when $z \to \pm\infty$. The same type of definition holds for the other electromagnetic fields (magnetic field, displacement field,…). By introducing into the Maxwell equations [13,14] the real fields under the form suggested by Eq. (1), and by imposing that the bulk fields fulfil these equations with the bulk dielectric functions $\varepsilon_{\pm}$, we are led to the following boundary conditions at the surface, i.e. of the bulk extrapolated fields:

$$[E_{\parallel}^{+}(r) - E_{\parallel}^{-}(r)]|_{z=0} = i\omega\hat{z} \times M_{\parallel}^{s}(r_{\parallel}) - \nabla_{\parallel} P_{z}^{s}(r_{\parallel}) \quad (2a)$$

$$[D_{z}^{+}(r) - D_{z}^{-}(r)]|_{z=0} = -\nabla_{\parallel} P_{\parallel}^{s}(r_{\parallel}) \quad (2b)$$

$$[H_{\parallel}^{+}(r) - H_{\parallel}^{-}(r)]|_{z=0} = i\omega\hat{z} \times P_{\parallel}^{s}(r_{\parallel}) - \nabla_{\parallel} M_{z}^{s}(r_{\parallel}) \quad (2c)$$

$$[B_{z}^{+}(r) - B_{z}^{-}(r)]|_{z=0} = -\nabla_{\parallel} M_{\parallel}^{s}(r_{\parallel}) \quad (2d)$$

where $\nabla_{\parallel}$ is the nabla operator parallel to the surface, subscripts $\parallel$ on vectors denote the projection of the vector into the *xy*-plane, while subscript z denotes the z-component of the corresponding vector [hence $r = (r_{\parallel}; r_z)$], ω is the optical frequency and $\hat{z}$ stands for the unit vector normal to the surface $z=0$. The various quantities that appear in Eq. (2a)–Eq. (2d) are the electric and magnetic fields, E and H, and the electric displacement and magnetic induction, D and B, respectively. In Eq. (2a)–Eq. (2d), total excess quantities denoted by superscripts s obtained by integrating the corresponding excess fields in the z-direction perpendicular to the surface were introduced:

$$D_{\parallel}^{s}(r_{\parallel}) = \int_{-\infty}^{\infty} dz D_{ex,\parallel}(r), \qquad E_{z}^{s}(r_{\parallel}) = \int_{-\infty}^{\infty} dz E_{ex,z}(r) \quad (3a)$$

and

$$B_{\parallel}^{s}(r_{\parallel}) = \int_{-\infty}^{\infty} dz B_{ex,\parallel}(r), \qquad H_{z}^{s}(r_{\parallel}) = \int_{-\infty}^{\infty} dz H_{ex,z}(r) \quad (3b)$$

Note that Eq. (2a)–Eq. (2d) can be obtained by gathering the integrated excess quantities in a singular Dirac term $\delta(z)$ located at the surface $(z=0)$ and by the imposition that fields such as:

$$E(r) = E^{-}(r)\theta(-z) + E^{s}(r)\delta(z) + E^{+}(r)\theta(z) \quad (4)$$

fulfil the Maxwell equations [7–9]. Likewise, to establish a complete link with the volume properties, the surface polarisation, $P^{s}(r_{\parallel})$, and magnetisation density, $M^{s}(r_{\parallel})$, are defined:

$$P^{s}(r_{\parallel}) = (D_{\parallel}^{s}(r_{\parallel}), -\varepsilon_0 E_{z}^{s}(r_{\parallel})),$$
$$M^{s}(r_{\parallel}) = (B_{\parallel}^{s}(r_{\parallel}), -\mu_0 H_{z}^{s}(r_{\parallel})) \quad (5)$$

where ε_0 and μ_0 are the electric permittivity and magnetic permeability in vacuum, respectively.

To proceed further, it is necessary to give constitutive relations characteristic of the interface that link the interfacial polarisation and magnetisation density $P^{s}(r_{\parallel})$, $M^{s}(r_{\parallel})$, and the extrapolated bulk fields at the surface. If the perturbed surface layer has a thickness smaller than the optical wavelength, all the excess fields are only non-negligible close to the surface. Thus, a local relation can be postulated. By purpose, the discussion will be restricted to non-magnetic material, which implies that $M^{s}(r_{\parallel}) = 0$. The simplest relation involves a symmetric constitutive interfacial tensor $\xi_{e}^{s}(\omega)$ [7,8]:

$$P^{s}(r_{\parallel}) = \xi_{e}^{s}(\omega)[E_{\parallel,\Sigma}(r_{\parallel}), D_{z,\Sigma}(r_{\parallel})] \quad (6)$$

where the index Σ defines the arithmetic mean of the corresponding bulk fields on both sides of the surface, i.e. $E_{\parallel,\Sigma}(r_{\parallel}) = \{E_{\parallel}^{+}(r_{\parallel}) + E_{\parallel}^{-}(r_{\parallel})\}/2$. For a homogeneous, isotropic and symmetric interface, $\xi_{e}^{s}(\omega)$ is diagonal:

$$\xi_{e}^{s}(\omega) = \begin{pmatrix} \gamma & 0 & 0 \\ 0 & \gamma & 0 \\ 0 & 0 & \beta \end{pmatrix} \quad (7)$$

The coefficients γ and β are called (first-order) surface susceptibilities, also referred as constitutive coefficients below, and describe the ability of the surface to polarise in the parallel or perpendicular directions. In fact, the spatial variations of the excess quantities have been implicitly forgotten, as only local relations between the total integrated surface polarisation gathered at the Fresnel surface and the bulk extrapolated fields have been chosen. These variations induce a non-local dependence, which is described by constitutive coefficients of second order, δ and τ [7,15]. These latter are d/λ smaller than the coefficients β and γ, where d is the thickness of the perturbed layer and λ is the optical wavelength.

Some invariants, independent of the choice of the reference Fresnel surface, can be defined as linear combinations of these four coefficients (β, γ, δ, τ); as the Fresnel quantities are independent of the choice of the separation surface, all the measurable Fresnel quantities can be uniquely expressed as a function of the invariants. However, even though all this theory is available in GranFilm, the following discussion is restricted to the first-order surface susceptibilities β and γ, which are the most important for metallic island layers. A full description of the invariants of the second-order coefficients and of the notion of stacking of films

that are beyond the scope of such an article can be found in [7].

2.2. The Fresnel coefficients

The calculation of the Fresnel coefficients in the two polarisation states *s* and *p* (see Fig. 1a) using only the surface susceptibilities can be found in [7,8,15,16] and follows the classical method developed in standard text books [13,14], except that the proper boundary conditions, Eq. (2a)–Eq. (2d), have to be taken into account, as well as the definition of the surface susceptibilities in Eq. (6).

The first consequence of this approach is that the surface perturbed layer characterised by the coefficients β and γ does not modify the classical Snell–Descartes relations [14] for the reflected and transmitted beams. Only the reflection, $r_\nu(\omega)$, and transmission amplitudes, $t_\nu(\omega)$, in polarisation $\nu = s,p$ are sensitive to the surface perturbation. In *s*-polarisation, we find:

$$r_s(\omega) = \frac{n_- \cos\theta_i - n_+ \cos\theta_t + i(\omega/c)\gamma}{n_- \cos\theta_i + n_+ \cos\theta_t - i(\omega/c)\gamma} \tag{8a}$$

$$t_s(\omega) = \frac{2n_- \cos\theta_i}{n_- \cos\theta_i + n_+ \cos\theta_t - i(\omega/c)\gamma} \tag{8b}$$

The angles of incidence θ_i, reflection θ_r and transmission θ_t defined in Fig. 1a and the bulk refractive index $n_\pm = \sqrt{\varepsilon_\pm}$ have been introduced in the previous equation. Note from Eq. (8a) and Eq. (8b) that the effect of the thin perturbed layer in *s*-polarisation only comes into play through the surface susceptibility, γ. Physically, this means that the incident *s*-polarised light can only excite modes parallel to the surface of the substrate. Furthermore, for *p*-polarisation we find:

$$r_p(\omega) = \frac{\kappa_-(\omega) - i(\omega/c)\gamma cos\theta_i \cos\theta_t + i(\omega/c) n_- n_+ \varepsilon_- \beta sin^2\theta_i}{\kappa_+(\omega) - i(\omega/c)\gamma cos\theta_i \cos\theta_t - i(\omega/c) n_- n_+ \varepsilon_- \beta sin^2\theta_i} \tag{9a}$$

$$t_p(\omega) = \frac{2n_- \cos\theta_i \left[1 + (\omega/2c)^2 \varepsilon_- \gamma\beta sin^2\theta_i\right]}{\kappa_+(\omega) - i(\omega/c)\gamma cos\theta_i \cos\theta_t - i(\omega/c) n_- n_+ \varepsilon_- \beta sin^2\theta_i} \tag{9b}$$

where the following notation has been introduced:

$$\kappa_\pm(\omega) = [n_+ \cos\theta_i \pm n_- \cos\theta_t]\left[1 - \frac{\omega^2}{4c^2}\varepsilon_- \gamma\beta sin^2\theta_i\right] \tag{9c}$$

We observe from Eq. (9a)–Eq. (9c) that a *p*-polarised beam incident upon a thin perturbed surface layer can activate both types of excitation, parallel and perpendicular to the surface. As usual, the reflection and transmission coefficients in energy are obtained from those in amplitude using conservation of the Poynting vector flux [13].

At this point, it is worth mentioning, even if it is not intended to discuss this in any detail, that similar formulas to Eq. (8a)–Eq. (9c) including the second-order coefficients δ and τ or the above-mentioned invariants have been derived [7,15] and are available in the GranFilm distribution.

3. Surface susceptibilities of island layers

So far, the discussion has been kept at a general level, and nothing was assumed regarding the geometry of the perturbed layer. This section focuses on a special important case, that of thin island films.

3.1. Optical response of nm-sized islands

For a thin and continuous film of thickness *d* and of dielectric function $\hat{\varepsilon}$, the surface susceptibilities are given by:

$$\gamma = d(\hat{\varepsilon} - \varepsilon_-), \qquad \beta = d\frac{\hat{\varepsilon} - \varepsilon_-}{\hat{\varepsilon}\varepsilon_-} \tag{10}$$

However, for thin, discontinuous films made of nm-sized islands supported on a substrate, the situation is far more complicated. This type of film, which corresponds to a so-called Volmer–Weber growth mode [1], is often encountered in experiments, in particular for metal deposits on dielectric substrates. The literature [5] on the optical properties of such systems is rich, perhaps because of the ease of measuring the Fresnel coefficients or because of the interest driven by the study of plasmon excitations in nanoparticles.

However, from a theoretical point of view, the most frequently used models to interpret the data are based on simplified approximations. The most common are: (i) the effective medium theories of Maxwell Garnett [17] or Bruggeman [6], in which the particles are assumed to be embedded into a host matrix with a dielectric function given by a Lorentz–Lorenz formula; or (ii) a pure dipolar model for simple island shapes, such as supported spheroid (Yamaguchi model [7,18–20]). The limitation of such models lies in the validity of the approximations used and/or in the description of the system geometry. Even though simplified models like the Yamaguchi dipolar model include the essential features of the island polarisability [20], they are not able to reproduce accurately the experimentally obtained optical spectra, as they do not properly account for the double break in symmetry, that of the particle truncation and that induced by electromagnetic coupling with the substrate.

The description of such phenomena needs a high number of multipoles, in particular to handle correctly the singularities of the electric field in the sharp corners of supported particles. In fact, many charge vibration channels for light absorption are allowed; their dynamic

charge localisations are mainly of dipolar and quadrupolar character [21–23] (see Section 5). Hence, in order to describe better the optical response of islands of various geometries, the exact island polarisabilities, both parallel, $\alpha_{\parallel}$, and perpendicular, $\alpha_{\perp}$, to the substrate have to be computed by taking into account multipolar coupling with the substrate. Indeed, if the islands are much smaller than the optical wavelength, the Rayleigh scattering cross-section [5,6] is negligible compared to the absorption. The surface polarisation density $P^s(r_{\parallel})$ is then mainly related to the number of islands per unit of surface ρ and to their ability to react to an applied field, i.e. their polarisability. The formal relations [7,11,12,24] between the surface susceptibilities and the island polarisabilities are in fact:

$$\gamma = \rho\alpha_{\parallel}, \qquad \beta = \rho\alpha_{\perp} \tag{11}$$

The full analytic and exact theory for the Rayleigh scattering by a particle with a diameter comparable to the wavelength of the incident radiation was originally obtained for an isolated sphere by Mie [25] in 1908. However, when the island, spherical or not, is supported by a substrate, the situation is much more difficult to handle [26] and is beyond the scope of the surface susceptibilities model described herein.

3.2. Computing the island polarisabilities

The optical properties of a layer made of sub-wavelength-sized islands are essentially driven by the particle polarisability. Thanks to the use of the discrete dipole approximation (DDA) [27], any type of particle shape can, in principle, be treated with today's modern computers, but often with high computational costs. However, simple island geometries, which result in much less computer-intensive calculations, are tractable by a different approach. From a practical point of view, two particle shapes that encompass a great number of experimental situations have been theoretically treated and are included into the GranFilm software: (i) the truncated sphere model [7,21,28–32] (see Fig. 1b); and (ii) the truncated oblate or prolate spheroid model [7,20,33], which includes shapes ranging from discs to needles.

The basic idea of the theoretical treatment is to solve the Laplace equation $\nabla^2\Psi(r)=0$ for the electrostatic potential $\Psi(r)$ as the quasi-static limit of the Maxwell equations is valid for sub-wavelength-sized islands. By using the particle symmetry, $\Psi(r)$ can be expanded on a multipolar basis in either spherical or spheroidal coordinates, depending on the shape of the island. The centre of expansion (see Fig. 1b) is located in the centre of the particle $\mathscr{O}$ or can freely move along the (vertical) symmetry axis. The surface of the substrate is handled by the classical charge image technique [13] using an image expansion point $\mathscr{O}'$, which is the mirror symmetric point of $\mathscr{O}$ with respect to the substrate. A clear distinction has to be made between emerging islands with $t_r = d/R > 0$ and caps for which $t_r < 0$ (see Fig. 1b). Wind et al. [29] put forward a technique to go from one case to the other by simply using symmetry arguments. We should, however, be aware that, strictly speaking, the expressions for the potential are formally different in the two situations [7].

In the expansion of the potential, for mathematical convenience, four separate media are assumed, as depicted in Fig. 1b, even though medium 4 is part of the substrate. For instance, for a truncated sphere, the expressions for the potential take the following form:

$$\Psi_1(r) = \Psi_0(r) + \sum_{lm}^{l\neq 0} A_{lm} r^{-l-1} Y_l^m(\theta,\phi) + \sum_{lm}^{l\neq 0} A^r_{lm} \rho^{-l-1} Y_l^m(\theta^r,\phi^r) \tag{12a}$$

$$\Psi_2(r) = \Psi^t_0(r) + \sum_{lm}^{l\neq 0} A^t_{lm} r^{-l-1} Y_l^m(\theta,\phi) \tag{12b}$$

$$\Psi_3(r) = \psi_0(r) + \sum_{lm}^{l\neq 0} B_{lm} r^l Y_l^m(\theta,\phi) + \sum_{lm}^{l\neq 0} B^r_{lm} \rho^l Y_l^m(\theta^r,\phi^r) \tag{12c}$$

$$\Psi_4(r) = \psi_0 + \sum_{lm}^{l\neq 0} B^t_{lm} r^l Y_l^m(\theta,\phi) \tag{12d}$$

where (r,θ,ϕ) and (ρ,θ^r,ϕ^r) are the spherical co-ordinates of a point in a frame centred in $\mathscr{O}$ and $\mathscr{O}'$, respectively (see Fig. 1b). In Eq. (12a)–Eq. (12d) the spherical harmonics [13] $Y_l^m(\theta,\phi)$ come into play, while A_{lm}, B_{lm}, A^r_{lm}, B^r_{lm}, A^t_{lm} and B^t_{lm} are the unknown multipolar expansion coefficients. Moreover, $\Psi_0(r)$ is the applied incident field, while $\Psi^t_0(r)$ represents the field transmitted directly into the substrate. As the expressions of Eq. (12a)–Eq. (12d) are purposely defined as solutions of the Laplace equation, the next step consists of writing the proper boundary conditions at each interface. These are the continuity of the potential itself $\Psi(r)$ and of the normal displacement field $\varepsilon(\omega)\partial_n\Psi(r)$, where $\partial_n = \hat{n}\cdot\nabla$ is the normal derivative at an interface of unit normal $\hat{n}$. The frequency-dependent complex dielectric constant $\varepsilon(\omega)$ of each medium is used, as the electric field is supposed to have a wavelength greater than the size of the particle and to oscillate at the optical frequency ω. The substrate surface boundary is automatically handled by the image charge method [13]:

$$A^r_{lm} = (-1)^{l+m}\frac{\varepsilon_1-\varepsilon_2}{\varepsilon_1+\varepsilon_2}A_{lm} \quad \text{and}$$

$$A^t_{lm} = \frac{2\varepsilon_1}{\varepsilon_1+\varepsilon_2}A_{lm} \tag{13a}$$

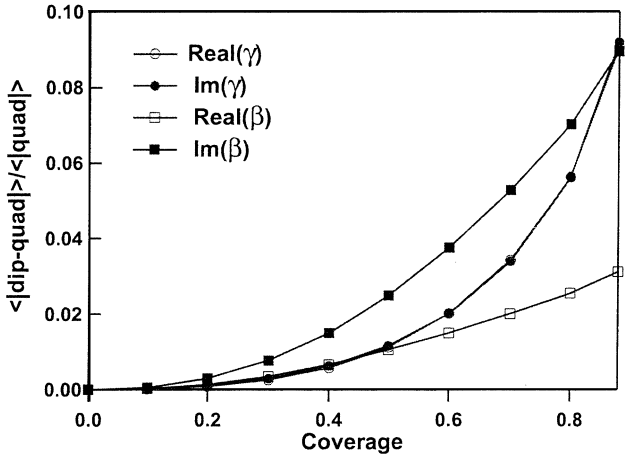

Fig. 2. Maximum relative errors for the surface susceptibilities (or the island polarisabilities) vs. coverage between the dipolar (dip) and quadrupolar (quad) inter-particle coupling approximations. The layer is made of hemispheres of Ag/MgO placed on a hexagonal lattice and the number of multipoles used in computing the island polarisabilities is $M=16$. The spectral range probed covers all the main features of the polarisabilities ($1.5<E<5$ eV). Note that the real and imaginary parts of γ are almost on top of each other.

$$B^r_{lm}=(-1)^{l+m}\frac{\varepsilon_3-\varepsilon_4}{\varepsilon_3+\varepsilon_4}B_{lm} \quad \text{and}$$

$$B^t_{lm}=\frac{2\varepsilon_3}{\varepsilon_3+\varepsilon_4}B_{lm} \tag{13b}$$

The usual way to treat the surface of the sphere is to use the orthogonality of the spherical harmonics $Y^m_l(\theta,\phi)$ as functions of the (θ,ϕ) angles. This method, called weak formulation of the boundary conditions, leads to two infinite linear systems for the multipolar coefficients A_{lm},B_{lm} for $m=0, \pm 1$. Indeed, each value $m=0, \pm 1$ corresponds to a peculiar symmetry state, i.e. a peculiar direction of the incident electric field (perpendicular or parallel to the surface of the substrate). Note that, for computing higher-order polarisabilities that are necessary when quadrupolar coupling between islands has to be treated (see Section 3.3), the $m=\pm 2$ system is useful. The linear systems, which can be found in [28,29,32], involve: (i) the various dielectric constants; and (ii) integrals of the spherical harmonics and their derivatives. The right-hand side corresponds to the external applied field. The polarisabilities are given by the first coefficients of the multipolar expansion in medium 1: $\alpha_\perp \simeq A_{10}$, $\alpha_\parallel \simeq A_{11}$. From a numerical point of view, the linear systems are solved for each wavelength or energy by truncating at an arbitrary multipolar order M. The convergence [32] upon increasing M is tested in two ways: (i) by simply looking at the convergence of the first term of the multipolar expansion, i.e. the island polarisability; and (ii) by post-checking the validity of the computed potential, i.e. by checking the boundary conditions on the potential itself and on the normal displacement at the surface of the sphere or spheroid. The second method is far more stringent than the first, as it tests all the potential validity. Most of the time, a value of $M=16$ is sufficient, but some situations are sometimes very slowly converging (like spherical caps or full spheres supported on a substrate) and are limited by machine accuracy.

3.3. Inter-island electromagnetic coupling

Of course, the islands are not isolated and react in a collective way to the applied field. The coupling between adjacent particles can also be treated in the quasistatic approximation if the separation between islands is much smaller than the optical wavelength, i.e. if the islands are excited by approximately the same amplitude. In the dipole approximation, the particles are submitted to the incident exciting field and to the local field resulting from the excited dipoles inside the particles and their images in the substrate. For emerging particles ($t_r>0$), the polarisabilities are in fact renormalised by the dipolar coupling in an analogous way to the Yamaguchi model [7,18,29,34,35]:

$$\alpha^I_\perp=\frac{\alpha_\perp}{1-2\alpha_\perp I^{20}_\perp}, \qquad \alpha^I_\parallel=\frac{\alpha_\parallel}{1+\alpha_\parallel I^{20}_\parallel} \tag{14}$$

where $\alpha_\perp$ and $\alpha_\parallel$ denote the polarisabilities of an isolated cluster in interaction with the substrate and are calculated as described in Section 3.2. The interaction functions $I^{20}_{\perp,\parallel}$ are defined by:

$$I^{20}_\perp=\frac{1}{\sqrt{20\pi}L^3\varepsilon_-}\left[S_{20}-\left(\frac{\varepsilon_--\varepsilon_+}{\varepsilon_-+\varepsilon_+}\right)\tilde{S}^r_{20}\right] \tag{15a}$$

$$I^{20}_\parallel=\frac{1}{\sqrt{20\pi}L^3\varepsilon_-}\left[S_{20}+\left(\frac{\varepsilon_--\varepsilon_+}{\varepsilon_-+\varepsilon_+}\right)\tilde{S}^r_{20}\right] \tag{15b}$$

and the direct and image lattice sums S_{20} and S^r_{20} by:

$$S_{20}=\sum_{i\neq 0}\left(\frac{L}{r}\right)^3 Y^0_2(\theta,\phi)\big|_{r=R_i} \tag{16a}$$

$$S^r_{20}=\sum_{i\neq 0}\left(\frac{L}{r}\right)^3 Y^0_2(\theta,\phi)\big|_{r=R_i{}^r} \tag{16b}$$

S_{20} describes the interaction with the others direct dipoles placed at $r=R_i$, whereas the effect of image dipoles at $r=R^r_i$ is included in S^r_{20}. L is the lattice parameter of the dipole lattice. Random arrays of dipoles can also be used [7]. Note that the term $i=0$ is excluded from the summation, as the polarisability α is that of an island interacting with the substrate. Going to higher order in the coupling between islands is rather complex for truncated particles, and implies the calculation of higher-order particle polarisability. For supported spheres, the problem is tractable to an arbitrary order [30], whereas for truncated particles, the calculation is

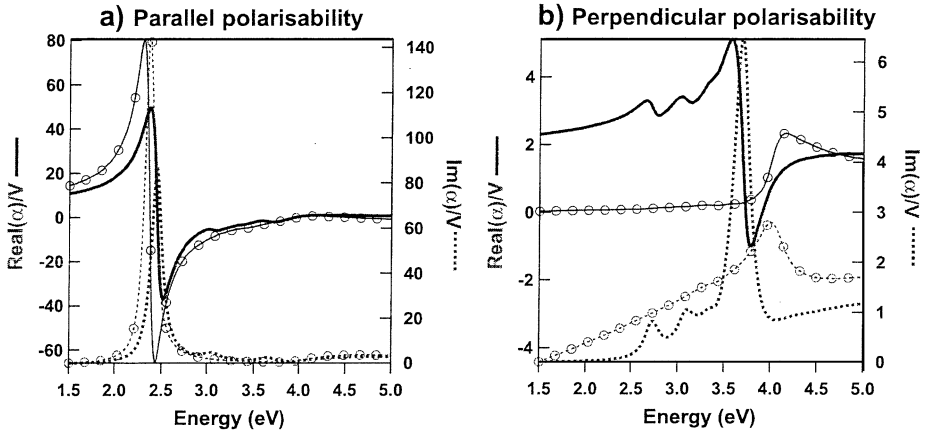

Fig. 3. Computed polarisabilities (a) parallel and (b) perpendicular to the surface of the substrate, for (i) (*bare lines*) a layer made of hemispherical islands of radius $R=8$ nm and (ii) (*line with circles*) a full-revolution ellipsoid lying on the substrate with the same radius $R=8$ nm and the same aspect ratio. The islands made of Ag are supported by a MgO substrate and cover 50% of the surface. In case (i), the polarisabilities have been computed up to $M=16$ multipolar order, accounting for the exact particle geometry, whereas in case (ii) the simplest pure dipolar Yamaguchi model was used. The bare polarisabilities have been corrected by a dipolar inter-particle coupling and normalised by the particle volume. The bulk dielectric functions have been used.

already lengthy up to quadrupolar order [7]. However, up to rather high surface coverage, which is higher than the interesting experimental limits, the differences between the two approximations are negligible. This was demonstrated in the case of supported spheres [30]. For truncated particles, Fig. 2 shows that the discrepancies in the surface susceptibilities or polarisabilities are minute up to 40% of coverage.

4. Software overview: computational methods and potentialities

The program GRANFILM, written in FORTRAN 90, is freely available for various platforms (Windows–Unix), in source as well as binary form; it can be downloaded with a brief user guide at http://www.phys.ntnu.no/~ingves/Software/GranularFilm/. GRANFILM deals with various types of surface layer geometries [7] with a thickness smaller than the optical wavelength:

i. Thin continuous film or stacking of films;
ii. Island layers made of truncated spheres or spheroids in multipolar coupling with the substrate [28,29,32,20];
iii. The Yamaguchi model for a spheroid interacting in a dipolar way with the substrate [18]; and
iv. Rough layers with a Gaussian height-correlation function [16].

GRANFILM is connected to a dielectric database, which allows handling of a great variety of materials, ranging from metals to semiconductors or dielectrics. Eventually, finite size corrections can be applied to the dielectric functions, in particular in the case of metals for which the plasmon oscillation lifetime τ is reduced by surface scattering [5,36]:

$$\varepsilon(\omega)=\varepsilon_{\mathrm{B}}(\omega)+\frac{\omega_{\mathrm{P}}^2}{\omega^2+i\omega\tau_{\mathrm{B}}^{-1}}-\frac{\omega_{\mathrm{P}}^2}{\omega^2+i\omega\tau^{-1}} \tag{17}$$

where ε_{B} is the bulk dielectric function, $\hbar\omega_{\mathrm{P}}$ is the plasma frequency and $\hbar/\tau_{\mathrm{B}}$ is the bulk relaxation time. A phenomenological dependence of the relaxation time upon the cluster size R' with a prefactor A that describes the interface damping [37] can be accounted for:

$$\frac{1}{\tau}=\frac{1}{\tau_{\mathrm{B}}}+A\frac{v_{\mathrm{F}}}{R'} \tag{18}$$

The available simulation outputs as a function of energy or optical wavelength at a fixed angle of incidence and given polarisation state are:

1. The surface susceptibilities;
2. The Fresnel coefficients (reflection, transmission or absorption) with both amplitude and phase;
3. The differential signals obtained by dividing the Fresnel quantities by that of the perfectly flat surface; and
4. The electron energy loss cross-section in reflection.

The main part of the program is to treat the island case. As discussed in the first part of this paper, the key ingredient for determining the surface susceptibilities is to obtain the island polarisabilities. These are computed in the quasistatic approximation by a multipolar expansion of the potential using the image charge technique. The matrix system, obtained using the weak formulation of the boundary conditions, is solved using the LU-decomposition algorithm of Slatec [38]. This part of the calculation is eventually performed in multiple precision [39] to reduce numerical round-off errors. The integrals needed to define the matrix elements are computed up to the desired accuracy using an auto-adaptive Gauss–

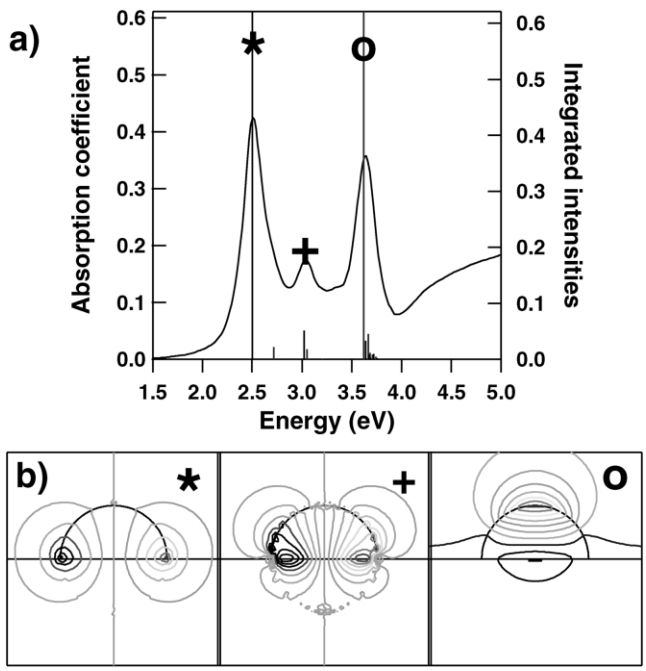

Fig. 4. (a) The absorption spectrum associated with the island layer morphology used in Fig. 3 without inter-particle coupling. Note the presence of several structures denoted by symbols. (b) Potential maps of the associated multipolar modes showing the polarisation charges: (*) parallel dipole, (+) quadrupole, and (o) normal dipole.

Konrod method [38]. This method has the advantage of correctly handling the oscillatory behaviour of the Legendre functions, which are part of the integrand. These latter functions and their derivatives are evaluated by taking advantage of the stable recurrence formulae [40,41]:

$$F_l^m(z) = \frac{1}{l-m}\left[(2l-1)zF_{l-1}^m - (l-1+m)F_{l-2}^m\right] \quad (19a)$$

$$\frac{\mathrm{d}F_l^m}{\mathrm{d}z}(z) = \frac{1}{z^2-1}\left[lzF_l^m - (l+m)F_{l-1}^m\right] \quad (19b)$$

The same kinds of relations also hold for the Legendre functions of the first and second kind needed in the expansions of the potential in spheroidal co ordinates [20], i.e. for islands of spheroidal shape. The convergence of the model with respect to the multipole cut-off M can be assessed by post-computing the potential and checking the boundary conditions on the surface of the island. A simple mapping of the real or imaginary part of the potential is also possible within GRANFILM. For a more detailed description of the multipolar absorption modes [23], the eigenmodes of charge polarisation in the no-damping limit can be computed. The frequency of these eigenmodes appear as the zeros of the determinant of the matrix used to calculate the expansion coefficients, i.e. as the poles of the particle polarisabilities vs. frequency. The oscillator strengths and broadening of these resonances are computed using an expansion of the linear system up to first order in the energy shift from the eigenmode and in the damping. The polarisation charges are visualised by plotting the equipotential lines corresponding to the eigenvectors of the multipolar coefficients. The coupling between islands is accounted for up to dipolar or quadrupolar order for ordered square or hexagonal lattices, or for disordered structures.

5. Examples: metals on dielectric substrates

The Volmer–Weber growth mode [1,42], i.e. by islands, is often encountered when metals are deposited on a dielectric substrate because of the poor adhesion energy of metals on such surfaces. Since the reflection coefficient of such a substrate is very low in the UV-visible spectral range, a small amount of metal, even in the submonolayer range, can be detected by simple optical means, such as surface differential reflectance spectroscopy [21,31,43–46]. The main results of our previous works were to show [20,31,32]: (i) how the optical response is sensitive to the layer morphology, and in particular to the aspect ratio of the particles; and (ii) that it is possible to reproduce quantitatively the optical spectra, and thereby to obtain information about the layer morphology consistent with direct ex situ measurements.

5.1. Fresnel coefficients for Ag on MgO

Silver is a good candidate for optical experiments, since its plasmon oscillations are not damped by inter-band transitions [5]. Thus, small silver particles exhibit strong resonances of the electronic gas upon an applied field. This is exemplified in Fig. 3, which shows computed polarisabilities of nanometric hemispherical islands. Both components of the polarisability, parallel and perpendicular to the surface of the substrate, exhibit strong, damped oscillator behaviour characteristic of a dipole. However, the situation is somewhat more complex, since the polarisabilities actually involve a mixture of modes [21–23]. Each mode is associated with a channel of absorption, as illustrated in Fig. 4, and to a specific dynamic charge vibration pattern. The most intense oscillation is caused by a dipolar charge localisation, whereas the others with lower oscillatory strengths are essentially of quadrupolar character. To a large extent, the optical behaviour of islands on a non-absorbing substrate, such as MgO, are driven by these polarisabilities, as they are the main inputs in the modified Fresnel formulae, Eq. (8a)–Eq. (9c). The need to compute the exact island polarisabilities by correctly treating coupling with the substrate and the particle shape is illustrated in Fig. 3 through a comparison with the simplest dipolar Yamaguchi model [7,18,19]. In this

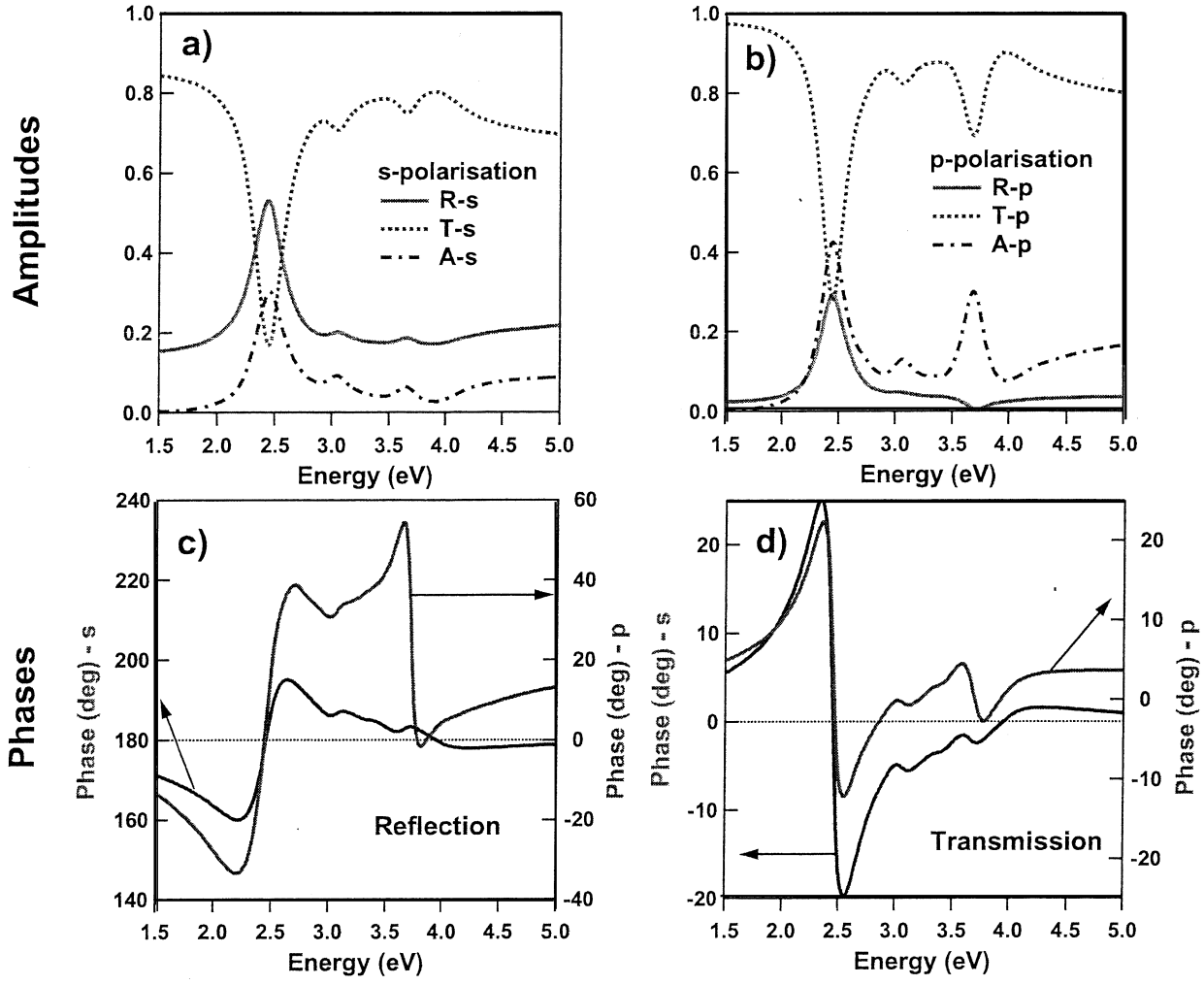

Fig. 5. Computed Fresnel coefficients (reflection–transmission–absorption) in (a) *s*-polarisation, (b) *p*-polarisation, and the phase factors in *s*,*p*-polarisations for (c) the reflection and (d) the transmission coefficients. The polarisabilities used are those of Fig. 3. The angle of incidence was set to $\theta_i = 45°$.

model, the island is replaced by a fictitious revolution ellipsoid, the polarisability of which is easily computed. The latter is then renormalised by the coupling with the image dipole inside the substrate. This fairly simple approach describes, in a pure dipolar way, the polarisation process of the island, but is unable to reproduce either the correct amplitudes or the correct energy positions for the absorptions [20]; attempts to use such a model to quantitatively analyse experimental data appear questionable [20].

Fig. 5 shows the optical coefficients for the two polarisation states $v = s,p$ of the incident light associated with the polarisabilities shown in Fig. 3 for an angle of incidence $\theta_i = 45°$. As a matter of comparison, the reflection for a bare MgO substrate is very low in the UV-visible spectral range (less than 3%) and nearly constant, since most of the light is transmitted. At first glance, all the Fresnel coefficients are very sensitive to the presence of the extra material at the interface. Even with just a thin deposited layer (3 nm) of a strong reflecting metal like silver, the reflectivity is considerably enhanced. The differences between *s*- and *p*-polarisations come from the fact that in the latter, the electric field is parallel to the incidence plane with two components parallel and perpendicular to the surface, whereas in *s*-polarisation, this vector is only parallel to the substrate surface. In *s*-polarisation, a dip in transmissivity appears at the resonance of the polarisability, a dip that is associated with an enhancement of reflectivity and an increase in the absorption of energy.

In *p*-polarisation, the two components of the polarisability can be excited, leading to two absorption peaks close to the particle resonance. The phase shift caused by the reflection or transmission is also affected by the presence of particles. Although it is not directly measurable, it comes into play in an ellipsometric measurement where the probed quantities, the ellipsometric coefficients $\Psi(\omega)$ and $\Delta(\omega)$, are defined through:

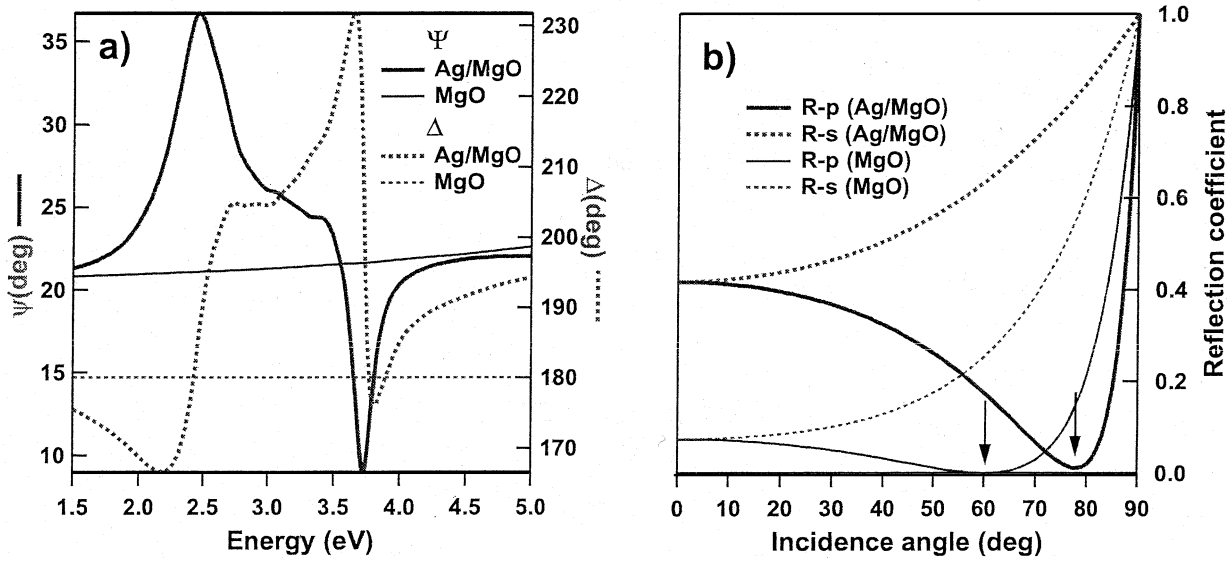

Fig. 6. (a) Calculated ellipsometric coefficients (i) for the bare MgO substrate (*thin lines*) and (ii) for an island layer with the same set of parameters as in Fig. 5 (*thick lines*). (b) Evolution with the incidence angle of the reflection coefficients in *s*,*p*-polarisations for Ag/MgO and MgO at the energy of the maximum of the parallel polarisability $E \approx 2.5$ eV (see Fig. 3). The Brewster angle θ_B is denoted by an arrow.

$$\rho(\omega) = \frac{r_p(\omega)}{r_s(\omega)} = \tan[\Psi(\omega)]\exp[i\Delta(\omega)] \qquad (20)$$

These ellipsometric coefficients, shown in Fig. 6, approximately reproduce the behaviour of the real and imaginary parts of the polarisability. The presence of the island layer also modifies the position of the Brewster angle θ_B at fixed energy (Fig. 6); at θ_B in *p*-polarisation, the reflectivity of MgO is equal to zero, whereas with silver islands, θ_B is strongly shifted and corresponds only to a minimum of the reflectivity.

Another common way of probing the dielectric properties of matter is to use electron energy loss spectroscopy in reflection geometry. The image field created by the moving electron leads to a dissipative process inside the surface layer. In an analogous way to the flat surface case [1], the cross-section of this phenomenon, $d^2\mathscr{S}/d(\hbar\omega)d\Omega$, was derived in the framework of sur-

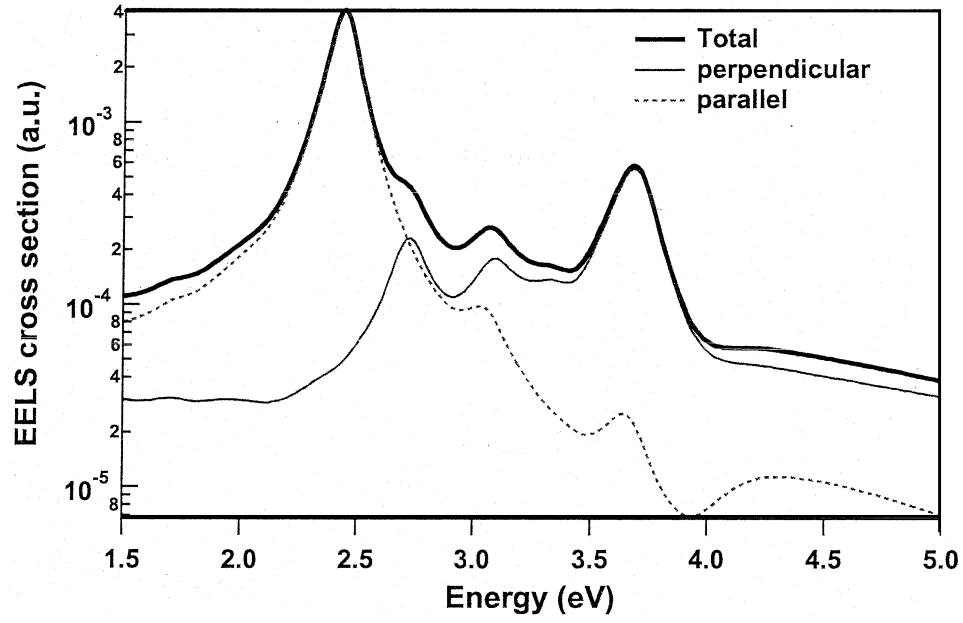

Fig. 7. Calculated electron-energy loss spectrum (EELS) for the Ag/MgO layer of Fig. 5. The incident electron energy is $E = 40$ eV and the parallel momentum transfer $k_{\parallel} = 0.003$ nm^{-1}. The parallel and perpendicular contributions to the EELS spectrum have been displayed separately, whereas the substrate contribution is negligible.

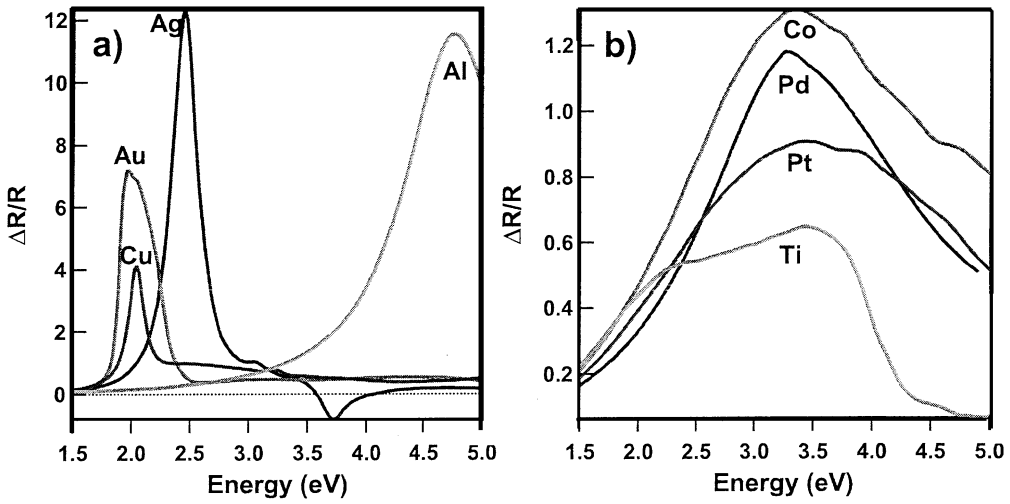

Fig. 8. Theoretical differential reflectance spectra for the same layer as in Fig. 5, but for various metals. (a) Noble or plasmon-free metals: Cu, Ag, Au and Al. (b) Transition metals: Ti, Co, Pd and Pt.

face susceptibilities in the limit of small momentum transfer:

$$\frac{d^2\mathscr{S}}{d(\hbar\omega)d\Omega} \sim \mathrm{Im}[\beta]\left|\frac{\varepsilon_2}{\varepsilon_1+\varepsilon_2}\right|^2 + \mathrm{Im}[\gamma]\left|\frac{1}{\varepsilon_1+\varepsilon_2}\right|^2 \quad (21)$$

Note that only the imaginary part of the surface susceptibility, i.e. absorption inside the islands, comes into play in the above equation. Fig. 7 shows the decomposition of the cross-section for the island layer of Fig. 3, with the two components parallel and perpendicular to the substrate. Of course, for the spectral range probed, MgO does not lead to any peculiar losses, as its bandgap is approximately 8 eV.

5.2. Plasmon-free metals vs. transitions metals

For alkali (Li, Na, K, Rb) or noble (Cu, Ag, Au) metals or aluminium (Al), the plasmon oscillations that appear when the real part of the dielectric function is close to zero, $\mathrm{Re}[\varepsilon(\omega_p)] \approx 0$, are poorly damped by the interband transitions. This means that, for such metals, the dominant contribution is an intraband collective behaviour described by a classical Drude model:

$$\varepsilon(\omega) = \varepsilon_{ib}(\omega) + \frac{\omega_P^2}{\omega^2 + i\omega\tau_B^{-1}} \quad (22)$$

and not by the interband contributions. In the above formula, ω_P is the plasmon frequency, τ_B is the relaxation time of the electrons, and $\varepsilon_{ib}(\omega)$ is the contribution of the interband transitions. In this case, the optical spectra for particles present sharp structures [31,45], the intensities and positions of which can be connected to the layer morphology. Fig. 8a illustrates this point for the differential reflectance spectra of Cu, Ag, Au and Al islands on a MgO substrate. The layer morphology is identical to that used in Fig. 5. For these metals, we can expect to extract, from optical measurements, quantitative information about the layer structure, i.e. radius, density and aspect ratio of the islands [20,31]. On the other hand, for transition metals, the dielectric behaviour

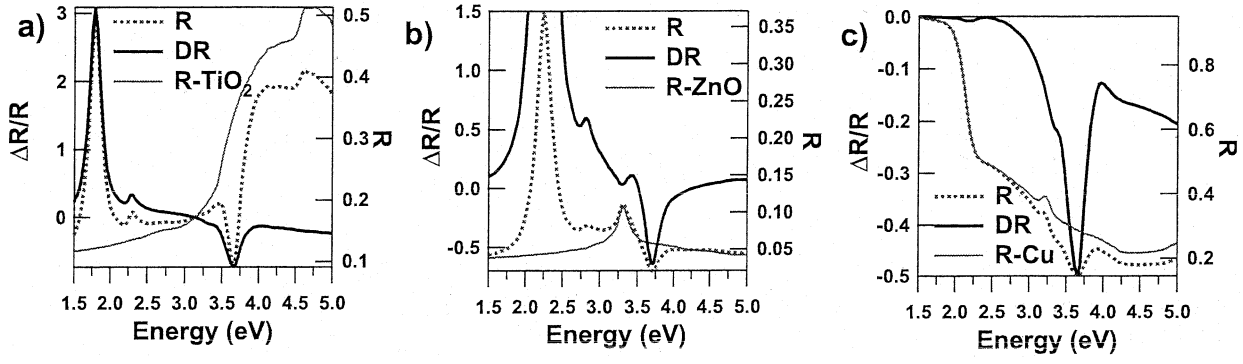

Fig. 9. The reflectivity R of a silver island layer (see Fig. 3 for the morphological parameters), the differential reflectivity $\Delta R/R$ and the bare substrate signal R-substrate in p-polarisation for three different absorbing substrates: (a) TiO_2; (b) ZnO; and (c) Cu.

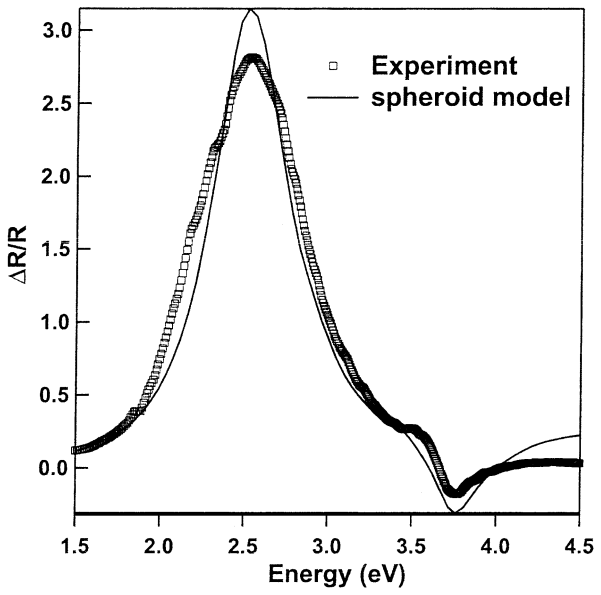

Fig. 10. Comparison between a theoretical fit using the GRANFILM program and an experimental differential reflectivity spectrum acquired during the growth of silver particles on magnesium oxide. The angle of incidence was set at $\theta_i = 45°$. The islands have been modelled by truncated spheroids for which polarisabilities have been computed at $M = 16$ multipolar order.

is far more complicated and, even though the electric field of an incident plane wave can polarise the electronic gas, the observed absorption structures are washed out by the interband transitions. Consequently, as illustrated in Fig. 8b in the case of Ti, Pd, Pt and Co, the spectra show a broad absorption band. In this case, the sensitivity of the optical response to the layer morphology is decreased and only qualitative conclusions can be drawn from an optical measurement [20].

5.3. Absorbing substrates

When the substrate is absorbing, the transmission coefficient is not well defined and the reflectivity spectra involve some extra features that are specific to the substrate. Fig. 9a,b show the optical spectra for an island layer of silver on two absorbing oxide substrates TiO_2 and ZnO. For TiO_2 and ZnO, the oxide gap is located in the UV-visible range (3.3 and 3 eV, respectively). The anisotropy of the substrate dielectric constant is sufficiently low to apply the above-described models. The bandgap absorption of ZnO is characterised by an exciton [47], which shows up clearly in the bare substrate reflectivity. This onset of bulk absorption should not be mistaken for the particle plasmon absorption, which is close in energy in the experimental spectra.

When the substrate is a metal like Cu [48] (see Fig. 9c), below the plasmon frequency, the reflectivity is high and drops quickly afterwards. If silver deposited on top of it forms islands, the parallel excitation is completely screened by the underlying metal; this can be understood in terms of cancelling of the parallel dipole moment by its perfect image in the metal. Only the perpendicular excitation is then visible.

5.4. Experimental results and GRANFILM

The usefulness of the surface susceptibilities approach and the sphere or spheroid island polarisability models were illustrated several times for various systems: Ag/TiO_2(110) [45], K/SiO_2/Si(001) [21], Ag/MgO(100) [20,31,32], Al–Ti–Ag/Al_2O_3(0001) [20,23], Au/TiO_2(110) or Au/Al_2O_3/NiAl(110) [49]. The agreement with the experimental optical spectra was always achieved with geometrical parameters (island radius and aspect ratio, island density) close to those found by imaging techniques. Fig. 10 shows the fit obtained with GRANFILM for a differential reflectivity spectrum acquired during the optical monitoring of evaporation of silver on a magnesium oxide substrate held at $T =$ 600 K under ultra-high vacuum. The experimental set-up and the growth conditions have been described elsewhere [32,20]. The Volmer–Weber growth mode of silver on oxide substrate and the high substrate temperature lead to the formation of nm-sized clusters, for which the shape is expected to be close to thermodynamic equilibrium i.e. spherical clusters. Ex situ imaging techniques and fit of the optical spectrum led to a similar mean island size of $R = 8.2$ nm and density $\rho = 1.9 \times 10^{11}$ cm^{-2}. The discrepancies between the broadness of the experimental and theoretical peaks can be attributed to the remaining size distribution, which was partially reduced by high-temperature growth. Accounting for this point will be a future improvement of the GRANFILM program.

6. Conclusion

The program GRANFILM and the underlying theoretical background of surface susceptibilities described in [7] are aimed as a tool for experimentalists for simulating and interpreting linear optical spectra taken on surfaces or thin films. The morphologies encompassed range from thin continuous films or rough surfaces to island layers made of truncated spheres or spheroids. The core of the program consists of computing the island polarisabilities accounting for the multipolar coupling with the substrate. Once done, all the linear Fresnel coefficients (reflection, transmission, absorption and ellipsometric quantities, and even electron energy loss cross-section) are accessible. Such simulations would be helpful, in particular to distinguish between the effect of particle shape on the optical response from that of the substrate or that linked to a pure modification of the particle dielectric constant.

Acknowledgments

The authors R.L. and I.S. would like to warmly acknowledge Dick Bedeaux and Jan Vlieger for having provided an unpublished version of their book [7] and for having shown a great enthusiasm in the development of GRANFILM.

References

[1] H. Lüth, Surface and Interfaces of Solids, Surface Science, Vol. 15, Springer Verlag, Berlin, 1992.
[2] P. Chiaradia, R. Del Sole, Surf. Rev. Lett. 6 (1999) 517.
[3] Y. Borensztein, Surf. Rev. Lett. 7 (2000) 399.
[4] D. Martin, P. Weightman, Surf. Rev. Lett. 7 (2000) 389.
[5] U. Kreibig, M. Vollmer, Optical Properties of Metal Clusters, Vol. 25, Springer Verlag, Berlin, 1995.
[6] C.F. Bohren, D.R. Huffman, Absorption and Scattering of Light by Small Particles, John Wiley & Sons, New York, 1983.
[7] D. Bedeaux, J. Vlieger, Optical Properties of Surfaces, Imperial College Press, London, 2001.
[8] D. Bedeaux, J. Vlieger, Physica A 67 (1973) 55.
[9] D. Bedeaux, J. Vlieger, Physica 73 (1973) 287.
[10] D. Bedeaux, J. Vlieger, Physica A 82 (1976) 221.
[11] A.M. Albano, D. Bedeaux, J. Vlieger, Physica A 99 (1979) 293.
[12] A.M. Albano, D. Bedeaux, J. Vlieger, Physica A 102 (1980) 105.
[13] J.D. Jackson, Classical Electrodynamics, Wiley & Sons, New York, 1975.
[14] M. Born, E. Wolf, Principles of Optics, 7th ed., Cambridge University Press, 1999.
[15] D. Bedeaux, G.J.M. Koper, E.A. Zeeuw, J. Vlieger, M. Wind, Physica A 207 (1994) 285.
[16] M.M. Wind, J. Vlieger, Physica A 125 (1984) 75.
[17] J.C. Maxwell Garnett, Phil. Trans. R. Soc. Lond. 230A (1904) 385.
[18] T. Yamaguchi, S. Yoshida, A. Kinbara, Thin Solid Films 18 (1973) 63.
[19] T. Yamaguchi, S. Yoshida, A. Kinbara, Thin Solid Films 21 (1974) 173.
[20] R. Lazzari, I. Simonsen, D. Bedeaux, J. Vlieger, J. Jupille, Eur. Phys. J. B 24 (2001) 267.
[21] C. Beita, Y. Borensztein, R. Lazzari, J. Nieto, R.G. Barrera, Phys. Rev. B 60 (1999) 6018.
[22] C. Noguez, R.G. Barrera, Phys. Rev. B 57 (1998) 302.
[23] R. Lazzari, S. Roux, I. Simonsen, J. Jupille, B. Bedeaux, V. Vlieger, Phys. Rev. B 65 (2002) 235424.
[24] M.T. Haarmans, D. Bedeaux, Thin Solid Films 258 (1995) 213.
[25] G. Mie, Ann. Phys. 25 (1908) 377.
[26] P.A. Bobbert, J. Vlieger, Physica A 137A (1986) 209.
[27] B.T. Draine, P.J. Flatau, J. Opt. Soc. Am. A 11 (1994) 1491.
[28] M.M. Wind, J. Vlieger, Physica A 141 (1987) 33.
[29] M.M. Wind, J. Vlieger, Physica A 143 (1987) 164.
[30] M.T. Haarmans, D. Bedeaux, Thin Solid Films 224 (1993) 117.
[31] R. Lazzari, J. Jupille, Y. Borensztein, Appl. Surf. Sci. 142 (1999) 451.
[32] I. Simonsen, R. Lazzari, J. Jupille, S. Roux, Phys. Rev. B 61 (2000) 7722.
[33] P.A. Bobbert, J. Vlieger, Physica A 147 (1987) 115.
[34] J. Vlieger, D. Bedeaux, Thin Solid Films 69 (1980) 107.
[35] R.G. Barrera, M. del Castillo-Mussot, G. Monsivais, Phys. Rev. B 43 (1991) 13819.
[36] H. Hövel, S. Fritz, A. Hilger, U. Kreibig, M. Vollmer, Phys. Rev. B 48 (1993) 18178.
[37] A. Hilger, N. Cüppers, M. Tenfelde, U. Kreibig, Eur. Phys. J. D 10 (2000) 115.
[38] http://www.netlib.org..
[39] D.M. Smith, Trans. Math. Softw. 17 (1991) 273.
[40] P.M. Morse, H. Feshbach, Methods of Theoretical Physics, Parts 1 and 2, MacGraw-Hill, New York, 1953.
[41] W.H. Press, S.A. Teukolsky, W.T. Vetterling, B.P. Flannery, Numerical Recipes in FORTRAN, Cambridge University Press, 1992.
[42] C. Henry, Surf. Sci. Rep. 31 (1998) 231.
[43] Y. Borensztein, R. Alameh, M. Roy, Phys. Rev. B 50 (1994) 1973.
[44] Y. Borensztein, M. Roy, R. Alameh, Europhys. Lett. 31 (1995) 311.
[45] D. Martin, J. Jupille, Y. Borensztein, Surf. Sci 377-379 (1997) 985.
[46] D. Martin, F. Creuzet, J. Jupille, Y. Borensztein, P. Gadenne, Surf. Sci. 377 (1997) 958.
[47] G.E. Jellison, L.A. Batner, Phys. Rev. B 58 (1998) 3586.
[48] Y. Borensztein, T. Lopez-Rios, G. Vuye, Phys. Rev. B 37 (1988) 6235.
[49] N. Nilius, N. Ernst, H.J. Freund, Phys. Rev. Lett. 84 (2000) 3994.